

Measurement of interstitial velocity of homogeneous bubbly flows at low to moderate void fraction

By V. ROIG AND A. LARUE DE TOURNEMINE

Institut de Mécanique des Fluides de Toulouse, UMR 5502 CNRS-INP-UPS,
Allée C. Soula, 31400 Toulouse, France

(Received 25 May 2005 and in revised form 23 June 2006)

We develop a new methodology to examine the conditional and unconditional vertical velocity induced by high-Reynolds-number bubbles rising in a uniform flow, at low to moderate void fraction α (up to 15 %). These statistics provide a local description of the perturbation of the liquid velocity around a test bubble in the swarm. In particular, the attenuation of the length of the wakes with increasing void fraction is measured for a large range of void fraction. The strong attenuation of the wakes is related to wake intermingling mechanisms. The methodology also enables a definition of the interstitial liquid flow. The velocity of the fluid averaged over all the interstitial volume far away from the bubbles is introduced. It is a useful concept, in particular to define the relative velocity, or for drift models. Our experimental results allow a discussion of the predictions of irrotational drift models. For low void fraction ($\alpha \leq 2\%$), potential flow models provide practical estimates of the interstitial velocity field. At higher void fractions, the effect of vorticity is important. A simple phenomenological model is proposed to include the effect of the flow generated by the bubble wakes.

1. Introduction

An important question for high-Reynolds-numbers bubbly flows is how to distinguish, in a meaningful way, between the flow generated locally by a bubble and the perturbations in the interstitial regions caused by bubble interaction. It is difficult to distinguish between velocity fluctuations caused by the wakes of bubbles and the near-field perturbation caused by the bubbles themselves. Our purpose is to obtain insight into the complex mechanisms of transport in the liquid phase of a bubbly flow, using precise and appropriate definitions of the statistical properties of the flow. The problem is addressed here for a homogeneous vertical flow perturbed by a uniform injection of ascending bubbles. In such a flow, in the absence of pre-existent turbulence, the random motions of the bubbles are responsible for all the random motions of the liquid. While recent experimental investigations have enhanced our comprehension of the behaviour of the fluctuations induced in bubbly flows (Zenit, Koch & Sangani 2001; Risso & Ellingsen 2002; Garnier, Lance & Marié 2002), there has been less work concerning the mean motion resulting from the anisotropy of the random movements induced in the liquid by the preferential alignment of the relative velocities of the bubbles with the vertical direction. In this work, we focus our attention on the generation of a mean motion in the liquid phase by the bubbles.

Recent studies devoted to the liquid motions induced in inertial bubbly suspensions have improved our knowledge of their dynamics. Risso & Ellingsen (2002) have given

a detailed experimental description of the statistical properties of the random motions in a homogeneous bubbly flow at low void fraction and high Reynolds number. They discussed the dependence of velocity statistics on the void fraction using conditional averages of the velocity field measurements. They disentangled the contributions to the velocity statistics of individual bubbles from those of hydrodynamic interactions, making use of the detailed characteristics of the reference flow around a single bubble discussed in Ellingsen & Risso (2001). The velocity disturbance induced by an isolated bubble is representative, at least at low void fraction α and in the neighbourhood of the bubble, of the velocity field induced in the vicinity of any individual bubble present in a swarm, whereas the flow field in the regions far away from the interfaces is determined by the hydrodynamic interactions. The effects of these interactions on the pair distribution function and on the bubble-induced motions in the liquid have been considered in particular by Koch (1993) and Esmaeeli & Tryggvason (1998, 1999). The dependence of the interactions on both the Reynolds number based on the relative velocity and on the void fraction has recently been discussed in Legendre, Magnaudet & Mougin (2003) for spherical particles.

In this contribution we present experiment results obtained in a uniform bubbly flow. At low enough void fraction, the local flow around any bubble is characterized by a Reynolds number $Re = U_R d_B / \nu$, and a Weber number, $We = \rho U_R^2 d_B / \sigma$ which is a measure of the bubble deformability (ρ , ν , σ , U_R and d_B are respectively the density and the viscosity of the liquid, the surface tension, the relative velocity and the diameter of the bubble). Interactions between bubbles depend on the decrease rate of the local perturbation induced by a bubble and on the void fraction α which controls the characteristic distance between the bubbles. Depending on the values of Re , We and α , a great variety of bubbly flows can therefore be observed. In this large domain, we focus on the analysis of inertial bubbly flows at large Re (typically $Re = 200$), and moderate We ($We = 0.4-0.6$), with void fractions up to 15%. Practical bubbly flow problems which occur in industry tend to be at void fractions in such a range. Moreover, there is a lack of concepts able to describe the velocity field in this case.

The present experimental work aims to contribute to the analysis of bubbly flows at moderate void fraction, using the idea that the global averaged dynamics of bubbly flows depend on the structure of the local flow around each bubble, which is strongly governed by the boundary conditions at its interface, as well as on the hydrodynamic interactions between the flow disturbances induced by each bubble. We therefore introduce a distinction between statistics conditioned or not by the presence of the bubbles. We have measured velocity signals obtained from one-point measurements by hot-film anemometry (HFA). These signals contain two interesting types of information: the alternation of phases at the measuring point, and the vertical velocity of the liquid when the tip of the probe is in the liquid. To our knowledge, these two kinds of signals have not been related often (except in Cartellier & Riviere 2001; Risso & Ellingsen 2002), and the coupling between the HFA velocity signal and the bubble passage signals has never been studied for void fraction above 2%. A schematic record of an HFA signal in the liquid perturbed by passing bubbles is shown on figure 1. Since we deal with complex bubbly flows at non-negligible void fraction, with moreover a dispersion of the bubble sizes, we have developed a specific methodology to reconstruct, from many HFA records, both the statistics of the local velocity field perturbed by an individual bubble, and the statistics of the interstitial velocity field.

The introduction of conditional statistics allows us to analyse the perturbation of the velocity of the liquid in the vicinity of the bubbles and the drift mechanisms.

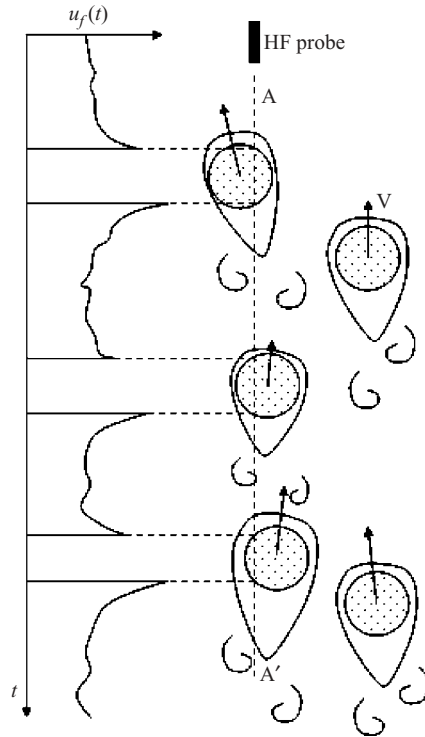


FIGURE 1. Partition of the liquid flow in: (i) a flow generated locally by each bubble, and (ii) the interstitial flow. We give a schematic correspondence between a velocity record $u_f(t)$ obtained from the HF probe immersed in a swarm and the bubble-induced liquid motions. The three bubbles crossing the probe along line AA' induce a strong perturbation in their vicinity. In order to identify the interstitial region, where hydrodynamic interactions are schematically shown, the extent of the local perturbation has to be estimated.

The pertinence of conditional averages appears clearly when defining an interstitial velocity to which a bubble responds, that is, when one is interested in the dynamics of the relative motion, or wishes to study the displacement of fluid induced by the relative motion. Kowe *et al.* (1988) first pointed out that the analysis of bubbly flows in terms of three velocity fields, respectively representative of the displaced liquid, of the interstitial liquid and of the bubbles, allows one to model a drift flux based on the mass conservation equation and to calculate the forces acting on the bubbles. Based on Darwin's analysis of the fluid displaced by an isolated sphere in potential flow, they developed a mechanistic drift flux model for bubbly flows taking into account added mass. They did not define precisely the interstitial average however.

In a recent study Eames *et al.* (2004) elaborated a precise concept of interstitial average. Our discussion of drift flux will thus focus on their analysis which revisited the concept of Darwin's inviscid drift and proposed new kinematic concepts which are useful for the characterization of the mean flow around groups of obstacles (see also Eames, Belcher & Hunt 1994 for a discussion of Darwin's drift). At present, vorticity is not taken into account in drift models predicting the liquid entrainment by isolated bubbles or in bubbly flows. Despite this shortcoming, irrotational models of drift provide a framework to analyse the effects of interactions on the modulation of the drift compared to the drift induced by an isolated bubble.

The paper is organized as follows. In §2, the experimental facility and instrumentation are presented. In §3, we introduce the various statistics used for the present analysis, and specifically the conditional time series of the velocity in the liquid. We describe the signal processing that has been developed in order to extract the characteristics of the velocity disturbance around each bubble. Then we explain how we split the liquid phase into a collection of volumes controlled by the presence of a test bubble, and another volume where the velocity field has lost the footprint of the bubble passage. Based on such a separation between a *near field*, and a *far field* away from the bubble, we define conditional statistics of the velocity field within the continuous phase. With these statistical tools we analyse the liquid flow inside the swarm of bubbles. The experimental results, their discussion and interpretation are given in §4. We show that the disturbance of the velocity in the liquid in the vicinity of the bubbles is strongly attenuated by wake interactions (§4.1). We then point out the differences between the various possible definitions of the relative velocity, which thus introduce different velocity scales for the relative movement (§4.2). Finally, we discuss how the conditional far-field averaged velocity can be used to analyse the mechanisms of mean liquid transport. A comparison of our measurements with existing irrotational drift flux models is discussed (§4.3), and an attempt to take into account the important effect of entrainment by the wakes is also discussed (§4.4).

2. Experimental methodology

2.1. Experimental apparatus and operating conditions

The experimental apparatus consists of a vertical channel in which the bubbly flows are manipulated at ambient temperature and pressure (figure 2) (for more details see Larue de Tournemine 2001). The injection device consists of a stagnation tank and a convergent section, both separated into two parts by a vertical splitter plate of 2.5 mm thickness. After the splitter plate the two bubbly flows mix in the vertical channel of 3.1 m height and $0.3 \times 0.15 \text{ m}^2$ cross-sectional area. Both sides of the tank are supplied independently with water and air. To generate bubbles, in each side of the convergent section 576 capillary tubes (80 cm long, 0.33 mm/1 mm internal/external diameter) are uniformly spaced on a grid and are distributed across the whole section of the channel ($0.15 \times 0.15 \text{ m}^2$ on each side). The tops of the capillary tubes are 2 cm below the top of the splitter plate. The two capillary tube networks are independently fed with air. Special care was taken to ensure there was no mean velocity gradient and no void fraction gradient at the inlet of the measurement channel. The liquid flow rate was fixed at $Q_L = 20 \times 10^{-3} \text{ m}^3 \text{ s}^{-1}$ for all the experiments, corresponding to a mean flow velocity of $\overline{U_{f0}} = 0.44 \text{ m s}^{-1}$ in single-phase flow. The gas flow rate was varied from $Q_G = 1.26 \times 10^{-4} \text{ m}^3 \text{ s}^{-1}$ to $Q_G = 1.8 \times 10^{-3} \text{ m}^3 \text{ s}^{-1}$, enabling the void fraction to be varied from 0.3 % to 14 %. Optical velocimetry techniques are limited to very low void fraction flows. For higher void fractions, optical measurements of the velocity field fail and we thus used hot-film anemometry. This is a reliable measurement technique if it is used with a non-negligible mean convective flow. On the other hand, in order to study a bubbly flow where all the fluctuating motions are generated by the relative motions of the bubbles, we had to inject bubbles in a very weakly turbulent flow with a turbulent intensity as low as possible. Thus we have chosen, as a compromise, the above liquid flow rate in order to generate, before bubble injection, a single-phase flow which is only weakly turbulent (the r.m.s. value of the velocity is $u'_{f0} = 8 \times 10^{-3} \text{ m s}^{-1}$).

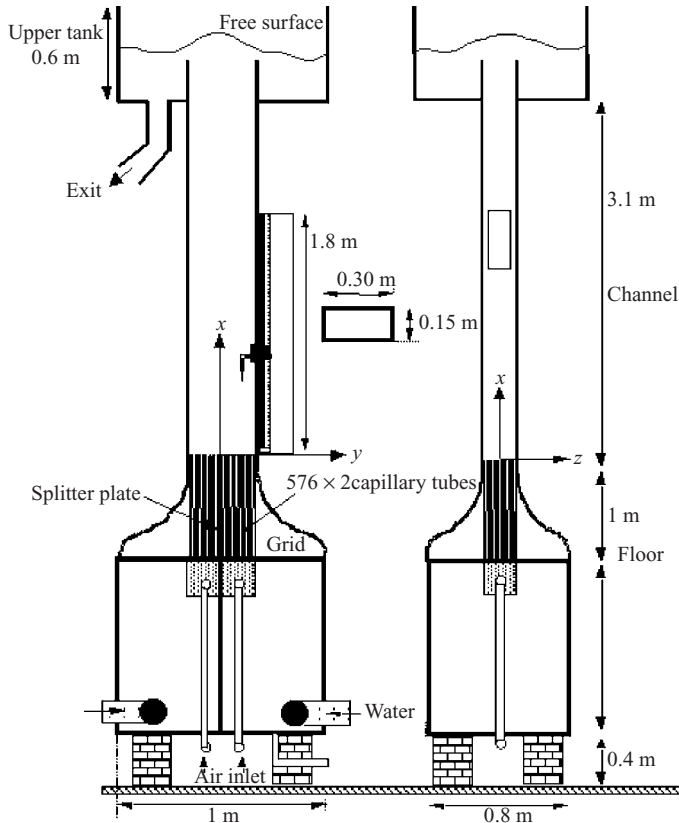


FIGURE 2. Experimental set-up.

This background flow, necessary to have acceptable measurements with a hot film, also serves to enhance the stability of the overall bubbly flow.

The bubble mean diameter d_B and the r.m.s. diameter d'_B were measured by double optical fibre probes (OFP) (see § 2.2). There is a limited polydispersion of the bubble sizes (d'_B/d_B is always lower than 15%). While the design of the bubble injection device ensures the temporal stability of the gas flow rate, it was not possible to fix the mean diameter of the bubbles at a constant value as α increases. Variation of the gas flow rate generates changes in the mean bubble diameter from 1.14 mm to 2.38 mm (figure 3) because of changes in detachment conditions at the tip of the capillary tubes. These variations of the bubble diameter with the void fraction mean that shape changes are expected. As d_B increases, the bubbles become more oblate. The aspect ratio χ defined by $\chi = a/b$, where a is the major axis length of the oblate bubble, and b its minor axis length, is given in figure 4. The values of χ were estimated by visual inspection of about 20 bubbles for five different void fractions between 0.7% and 5%. A mean diameter was also estimated from photographs (figure 3). The evolution of the aspect ratio of the bubbles with the void fraction is consistent with the empirical relation given by Duineveld (1995) for measurements of low deformable bubbles in water (figure 4). The change in bubble shape alters their dynamics. For an isolated bubble such a change in diameter and shape would lead to a modification of the trajectory from rectilinear to zigzag or helical. In our study, as the void fraction varies, the parameters involved in the liquid transport such as the

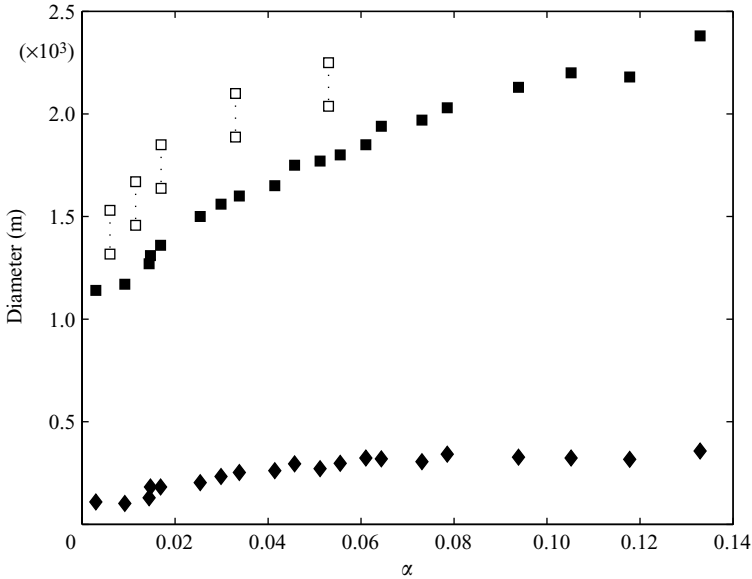


FIGURE 3. Size of the bubble: ■, mean diameter d_B ; ◆, r.m.s. diameter d'_B ; □····□, video estimation of d_B .

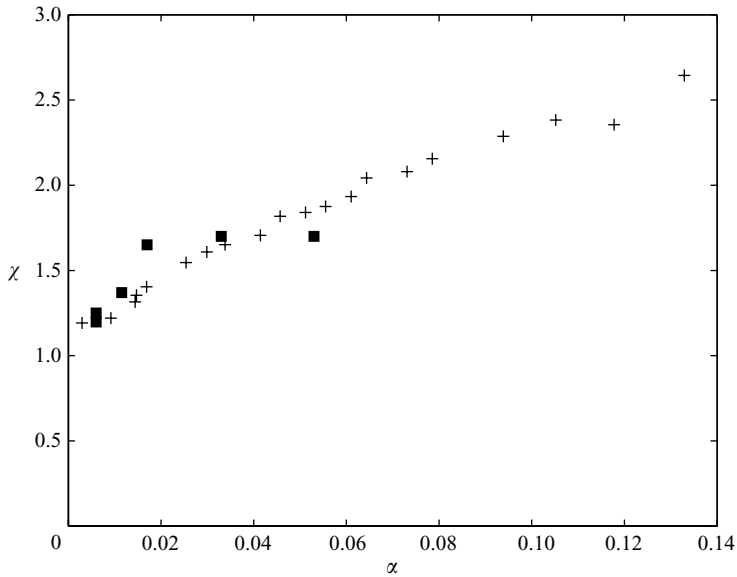


FIGURE 4. Aspect ratio of the bubbles: ■, video estimation of χ ; +, χ from Duineveld (1995) (when $d_B \leq 1.8$ mm in MKS : $\chi = \sqrt{d_B}/(0.0505 - 0.657\sqrt{d_B})$).

relative velocity and the added-mass coefficients are therefore not only modified by the void fraction, but also by the changes of shapes and equivalent diameters.

In our set-up, preliminary experiments on bubbly flows generated by a homogeneous injection have shown homogeneous distributions of liquid velocity and void fraction for $\alpha \leq 2\%$. For $\alpha > 8\%$, the void fraction profiles and liquid velocity profiles were not perfectly uniform, with the void fraction being slightly higher at the centre of the

measuring section. Measurements were taken at a fixed position (17 cm above the top of the splitter plate), far enough away from the splitter plate wake and the tank walls. In the vicinity of the measuring point, the flow is locally quasi-homogeneous because the spatial variations in the velocity field and void fraction occur over a larger scale. The results are reproducible, which was confirmed by considering other points farther from the splitter plate. This shows that the results are not affected by non-perfectly homogeneous experimental conditions.

2.2. Measuring methods

A calibrated hot-film anemometer (HFA) was used to measure the velocity of the liquid phase. The HFA was composed of a single cylindrical hot-film probe (Dantec, 55R11) and a constant-temperature anemometer (Dantec, Streamline 90N10). The overheat ratio was fixed at a low value (6%) to avoid bubble formation on the hot-film element by gas dissolution. The temperature of the water was maintained constant during the experiments because of the large thermal capacity of the tank from which water was pumped. The sampling frequency was chosen equal to 5 kHz, and measurements were recorded for at least 100 s. The accuracy of the liquid velocity was estimated by repeating the measurements and examining data scattering. The relative error is always lower than 5%. The diameter and length of the sensitive element of the probe (70 μm , 1.25 mm), associated with the non-negligible mean liquid velocity, allowed correct piercing of the bubbles, so that interactions between the probe and the bubbles were negligible (Bruun 1995; Serizawa, Tsuda & Michiyoshi 1983). The passing of a bubble over the film causes a sudden change in heat transfer, so that the associated portion of the signal has no meaning and must be removed from the signal (figure 5a). We used a phase discrimination algorithm described by Farrar *et al.* (1995) to separate the parts of the HFA signal related to the bubble passages. The algorithm is briefly discussed in the caption of figure 5 (for more details see Larue de Tournemine 2001). A comparison between simultaneous measurements of the liquid velocity using both a laser and a HFA at the same point confirms that both systems give the same velocity time series in the vicinity of a bubble passage, and that only the abrupt negative fall which characterizes the bubble presence on the film must be removed (Ellingsen *et al.* 1997).

An optical fibre probe was used to measure the void fraction. The fast response time of the probe (2 μs) allows the presence of the gas phase to be determined using a simple threshold method. A double optical fibre probe, consisting of elements separated by a vertical distance of 3.1 mm, was used to measure the bubble velocities, and their sizes (see Serizawa, Kataoka & Michiyoshi 1975, Clark & Turton 1988, Roig 1993 and Kamp 1996 for a description of the signal processing algorithms). The relative errors for the mean diameter of the bubbles and for the mean vertical velocity were estimated to be less than 6%.

3. Time series analysis

3.1. Definition of averaged velocities in both phases

The time series of the velocity $u(t)$ at a fixed point is equal to the velocity of the fluid $u_f(t)$ when the probe is in the continuous fluid phase. In a time series of duration T , we denote respectively t_{Ai} and t_{Di} as the times of arrival and departure of bubble i detected on the HFA signal (figure 5b). Using the Heaviside function $H(t)$ we define the elementary characteristic function for the presence of the fluid: $g_i(t) = H(t - t_{Di}) - H(t - t_{Ai+1})$ which is zero except for $t_{Di} \leq t \leq t_{Ai+1}$. The characteristic

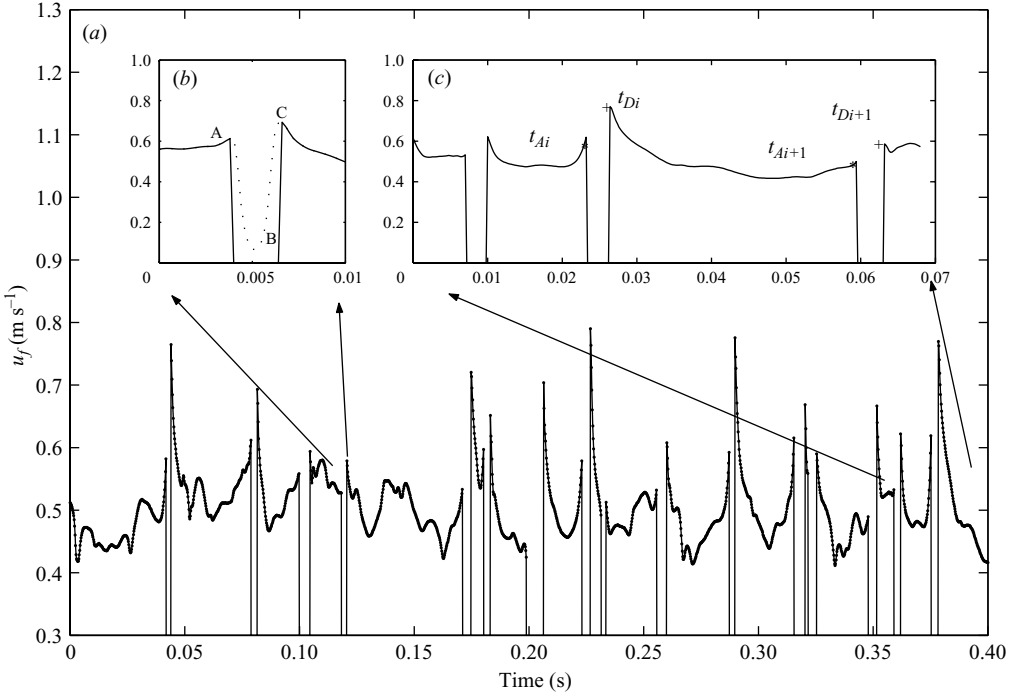


FIGURE 5. Typical signal obtained from hot-film anemometry: (a) record at $\alpha = 8\%$; (b) visualization of the three points (A, B, C) used for phase discrimination. Phase discrimination consists of identifying, from examination of the slope of the signal, the points A, B and C due to the bubble passage on the hot film. Point A is the front interface of the bubble, B is the rear interface. [BC] is the response of the anemometer to the rapid variation of thermal conditions associated with the dynamics of the liquid meniscus between the sensor and the bubble during the rear interface passage. While [BC] does not represent the continuous-phase velocity, the decrease after point C is representative of the liquid movement near the bubble. Thus, there is an undetectable liquid region in the very near field of any interface, but the extent of this field is negligible. (c) visualization of the reference times (t_{Ai} and t_{Di}) used for conditional averages.

function of the fluid phase is $\chi_f(t) = \sum_{i=1}^N g_i(t)$, N being the number of bubbles which have passed in time T . We thus define the velocity in the liquid phase by $u_f(t) = u(t)\chi_f(t)$.

The unconditionally averaged velocity in the liquid phase is then classically given by averaging over the whole record in the liquid phase

$$\overline{U_f} = \frac{\int_0^T u_f(t) dt}{\int_0^T \chi_f(t) dt}. \quad (3.1)$$

The mean velocity of the bubbles $\overline{V_B}$ has been defined as the statistical average of the velocities of the bubbles, with v_{Bi} the velocity of bubble i ,

$$\overline{V_B} = \frac{1}{N} \sum_{i=1}^N v_{Bi}. \quad (3.2)$$

The averaged velocity in the gas phase taking into account the residence time Δt_{Bi} of the bubbles, is defined as

$$\overline{U}_G = \frac{1}{\sum_i \Delta t_{Bi}} \sum_i \Delta t_{Bi} v_{Bi}. \quad (3.3)$$

The unconditionally averaged velocities in both phases, \overline{U}_f and \overline{U}_G , are used in most of the modelling approaches (Drew 1983; Biesheuvel & van Wijngaarden 1984).

3.2. Conditionally averaged velocities

The two types of information contained in the HFA signal – the vertical velocity of the liquid and the times of arrival/departure of the bubbles (figure 5a) – are used to define a measurement of the averaged vertical disturbance around a test bubble. We then introduce Eulerian conditional statistics for the vertical velocity field far away from any bubble.

3.2.1. Conditional time series of the velocity in the liquid

The averaged form of the vertical velocity field in the liquid phase in the neighbourhood of a bubble in the swarm is calculated from the following conditional time series. For the fluid velocity downstream of the bubbles we calculate

$$\langle u(\tau) \rangle_d = \frac{\sum_{i=1}^N u_f(t_{Di} + \tau) g_i(t_{Di} + \tau)}{\sum_{i=1}^N g_i(t_{Di} + \tau)} \quad (3.4)$$

which is defined for $0 \leq \tau \leq \max_i(t_{Ai+1} - t_{Di})$, where $\tau \geq 0$ is the time from the passage of the rear interface. In the same way, for the fluid upstream of the bubbles (for $\min_i(t_{Di-1} - t_{Ai}) \leq \tau \leq 0$, where $\tau \leq 0$ is the time before the bubble arrives), we introduce the conditionally averaged time series

$$\langle u(\tau) \rangle_u = \frac{\sum_{i=1}^N u_f(t_{Ai} + \tau) g_{i-1}(t_{Ai} + \tau)}{\sum_{i=1}^N g_{i-1}(t_{Ai} + \tau)}. \quad (3.5)$$

A schematic illustration of the method of calculating the conditionally averaged time series $\langle u(\tau) \rangle$ is given in figure 6 (where $\langle u(\tau) \rangle$ stands for $\langle u(\tau) \rangle_d$ or $\langle u(\tau) \rangle_u$). In the following, we will call the above definitions *unfiltered* conditionally averaged time series, because they include, through $g_i(t)$, disturbances due to neighbouring bubbles, which will be found to be important later.

We performed an Eulerian measurement at a fixed point of the time series $\langle u(\tau) \rangle$ of the disturbance of the liquid velocity due to the relative motion of the bubbles. To convert, in the vicinity of the bubbles, temporal information on the vertical velocity field into spatial information, we have applied a Taylor hypothesis (Hinze 1987), using the bubble mean rise velocity \overline{V}_B . The disturbance in the vicinity of the bubble being closely controlled by the boundary condition at its surface, we have assumed that the disturbance is transported at the velocity of the bubbles as in Cartellier & Riviere (2001). Strictly speaking, this hypothesis is valid if $\overline{V}_B \gg (\overline{V}_B - \overline{U}_f)$, which is

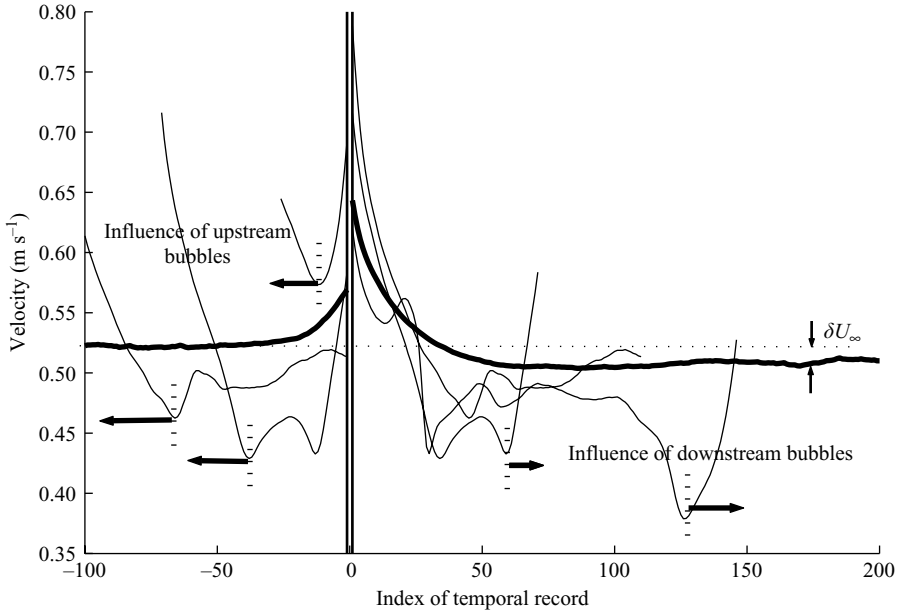


FIGURE 6. Calculation of the conditional time series. Some instantaneous records of the velocity in the liquid phase around bubbles are plotted. 0 corresponds to the bubble passage. For the *unfiltered* conditional average, plotted in bold, the average is taken over all the records around the bubbles including the parts of the signals (pointed out by arrows) associated with the influence of the neighbouring bubbles; this average thus results in a difference between the velocities at infinity denoted δU_∞ . We next introduce the *filtered* conditional average, not plotted here, for which the parts of the signals associated with the influence of the neighbouring bubbles are not taken into account, and δU_∞ then tends towards 0.

reasonably well satisfied in the present measurements ($0.2 \leq (\overline{V_B} - \overline{U_f})/\overline{V_B} \leq 0.3$). In such conditions, the time record of the disturbance at a fixed point is equivalent to the time record of a ‘frozen’ spatial disturbance crossing the point of measurement at velocity $\overline{V_B}$, and the time-to-space transformation is possible.

A characteristic of one-point measurements is that the averages are not spatial averages over the whole domain around a bubble, but are conditioned on the detection of the interface by the hot-film sensor (see figure 1). Our conditional averaging procedure averages all the contributions of the bubbles crossing the point of measurement, whatever the positions of their centres relative to the probe, and for all velocities and orientations of the oblate bubbles with respect to the vertical direction. The strength of the disturbance produced by a bubble passage and the preferential orientation of the trajectories towards the vertical direction are nevertheless strong enough for a statistically meaningful average to arise. We can consider that we measure a spatial conditional average over an approximate vertical cylinder of ellipsoidal cross-section intersecting the test bubble.

The *unfiltered* conditional averages of the vertical velocity $\langle u(\tau) \rangle$ are reported for different void fractions in figure 7. Up to $\alpha = 0.13$, the vertical velocity field induced by bubble passages has a well-defined averaged form revealing the local flow induced by bubbles. An important feature of our experimental conditional average is that to each side of the bubble, far away from the bubble interfaces, it reaches an asymptotic value, independent of the distance from the bubble. This far field is, thus, not controlled by the action of the test bubble.

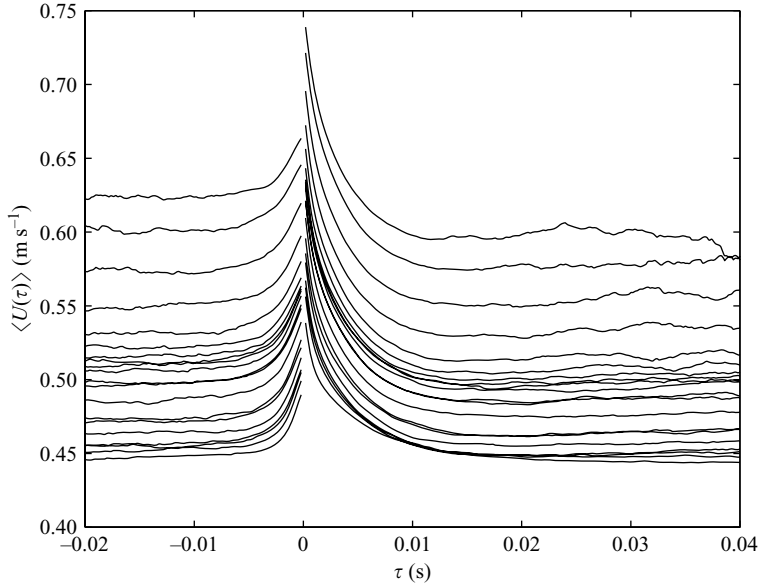


FIGURE 7. *Unfiltered* phase average of the liquid velocity around the bubbles. Time $\tau = 0$ corresponds to the interface passages, $\tau < 0$ to the region upstream of the bubbles, $\tau > 0$ to the downstream region of the bubbles. All runs for $0.3\% \leq \alpha \leq 13\%$. When α increases the curves are displaced to higher values.

However, it is important to notice that changes in the void fraction modify the values of the asymptotic far field of the unfiltered conditionally averaged time series (figure 7). The first effect of increasing the void fraction is to increase $\langle u(\tau) \rangle$. This global displacement is consistent with the increase of void fraction for a constant liquid flow rate. A more subtle effect of increasing the void fraction is related to the appearance of an asymmetry of the flow far from the interfaces. For low values of α , both upstream and downstream conditionally averaged perturbations relax asymptotically towards the same values at infinity on each side of the bubble. But for $\alpha > 2\%$ we obtain $\langle u(\tau \rightarrow +\infty) \rangle_d \neq \langle u(\tau \rightarrow -\infty) \rangle_u$. This is because the calculation of the unfiltered conditionally averaged fields around a bubble also includes the disturbance motion of that bubble as well as the influence of the velocity perturbations of the surrounding bubbles (figure 6). Because a wake develops at the rear of a bubble, the upstream average is systematically higher than the downstream average. At this step of the conditional average process, the estimated far field is thus not representative of a field *far away from any bubble*. The second effect associated with void fraction variation consists of a modification of the time and spatial scales necessary to recover the asymptotic external velocity values on each side of the bubble. A discussion of the underlying physics is given in §4.1.

While the primary unfiltered conditional average of the time series $\langle u(\tau) \rangle$ represents the mean flow around a bubble in a swarm, it is more relevant to define another conditional average that filters the direct influence of the neighbouring bubbles. This will allow a discussion of the differences between a region near any individual bubble in the suspension, which is mainly controlled by the boundary condition at this interface, and an external far field only influenced by the hydrodynamic interactions.

To calculate this new conditional average, denoted *filtered*, we use the time scales τ_{rd} and τ_{ru} of the perturbations obtained by fitting of the primary *unfiltered* conditional

averages by an exponential law (see § 4.1 for a physical justification of this fitting law and for a precise definition of τ_{rd} and τ_{ru}). To eliminate the direct influence of the neighbouring bubbles on the conditional time series we thus define the following elementary characteristic functions for the fluid in the vicinity of a bubble:

$$\tilde{g}_{d,i}(t) = H(t - t_{Di}) - H(t - t_{Ai+1} + \tau_{ru})$$

which is zero except for $t_{Di} \leq t \leq (t_{Ai+1} - \tau_{ru})$, and similarly

$$\tilde{g}_{u,i}(t) = H(t - t_{Di-1} - \tau_{rd}) - H(t - t_{Ai}).$$

For the fluid velocity in the vicinity of the bubbles we thus calculate the *filtered* conditionally averaged time series

$$\langle \tilde{u}(\tau) \rangle_d = \frac{\sum_{i=1}^N u_f(t_{Di} + \tau) \tilde{g}_{d,i}(t_{Di} + \tau)}{\sum_{i=1}^N \tilde{g}_{d,i}(t_{Di} + \tau)} \quad (3.6)$$

which is defined for $0 \leq \tau \leq \max_i(t_{Ai+1} - \tau_{ru} - t_{Di})$; and in the same way, for $\min_i(t_{Di-1} + \tau_{rd} - t_{Ai}) \leq \tau \leq 0$,

$$\langle \tilde{u}(\tau) \rangle_u = \frac{\sum_{i=1}^N u_f(t_{Ai} + \tau) \tilde{g}_{u,i}(t_{Ai} + \tau)}{\sum_{i=1}^N \tilde{g}_{u,i}(t_{Ai} + \tau)}. \quad (3.7)$$

The global shape of the filtered conditionally averaged time series (denoted $\langle \tilde{u}(\tau) \rangle$) for both positive and negative values of τ is not very different from the unfiltered ones, neither are their associated relaxation times (figure 8). But the values at infinity on both sides of the bubble are now identical. This proves that excluding near fields from conditional calculations leads to a well-defined unique behaviour at infinity. The small differences between filtered and unfiltered averages, except at infinity, can be related to the exclusion effect in the wakes of the bubbles, which will be discussed later, and to the shortness of the upstream disturbance.

We can finally conclude that, even if the void fraction is not negligible, the values of the relaxation lengths that we can calculate from the *filtered* conditional average procedure are representative of the size of a local perturbation controlled by the motion of an individual bubble. And that outside of this zone, we can measure a velocity field that is independent of this perturbation and results from the collective interactions in the suspension.

3.2.2. Definition of conditional averages

Because upstream and downstream conditionally averaged perturbations relax towards the same values at infinity, we can define clearly a unique asymptotic far field, and introduce conditional statistics in the region far away from the bubbles.

We define the elementary characteristic function for the fluid far away from any bubble as

$$g_{FF,i}(t) = H(t - t_{Di} - \tau_{cut,d}) - H(t - t_{Ai+1} + \tau_{cut,u}).$$

The values of $\tau_{cut,d}$ and $\tau_{cut,u}$ fix the size of an exclusion zone around the bubbles and are related to τ_{rd} and τ_{ru} . Function $g_{FF,i}(t)$ exists only if $(t_{Di} + \tau_{cut,d}) < (t_{Ai+1} - \tau_{cut,u})$.

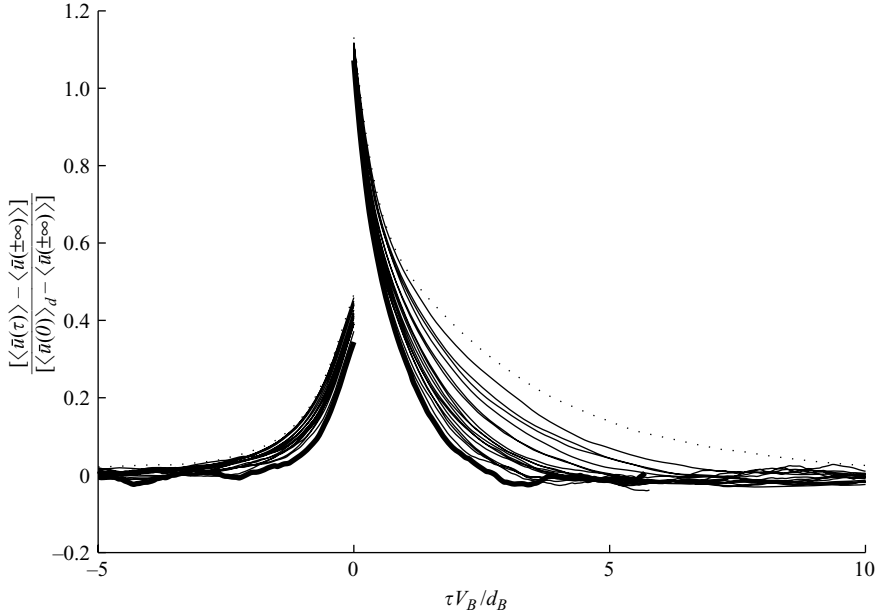


FIGURE 8. Filtered phase average of the liquid velocity around the bubble (dotted line: minimum void fraction; bold line: maximum void fraction). All runs for $\alpha \leq 13\%$. When α increases, the rear perturbations ($\tau > 0$) attenuate faster.

The characteristic function of the fluid phase in the far field of any bubble is

$$\chi_{FF}(t) = \sum_{i=1}^N g_{FF,i}(t).$$

The velocity of the liquid in the far field of any bubble is thus $u_{FF}(t) = u(t)\chi_{FF}(t)$.

The conditionally averaged velocity of the fluid in the far field is then

$$\overline{U_{FF}} = \frac{\int_0^T u_{FF}(t) dt}{\int_0^T \chi_{FF}(t) dt}. \quad (3.8)$$

In the following, we present arguments supporting the ability of our methodology to provide a well-defined conditional measurement of the velocity in the far field of any bubble present in a swarm at moderate α . We also discuss the limits in the void fraction range for such a methodology to apply.

In order to measure the far field statistics, $\tau_{cut,d}$ and $\tau_{cut,u}$ must be carefully chosen. Their values have been selected in a range so that the conditional statistics in the far field are not dependent on the choice of $\tau_{cut,d}$ and $\tau_{cut,u}$. The value of $\overline{U_{FF}}$ is not sensitive to the choice of these relaxation times if they are long enough to allow removal of the most important part of the bubble-induced disturbance (Larue de Tournemine 2001). (They are defined more precisely from (4.2) with β taken equal to $\beta_d = 10^{-4}$ and $\beta_u = 5 \times 10^{-4}$ respectively).

It is also crucial to assess whether $\overline{U_{FF}}$ obtained from one-point measurements is representative of the liquid velocity averaged over all the interstitial far-field volume around the bubbles, and not only in the interstitial volume. The probability of

considering as a far-field event a near-field event associated with a bubble passing in the vicinity of the point of measurement, but that would not have been detected by the probe, is low (proportional to α^2 (Batchelor 1972)). Thus, our method of distinguishing between near field and far field from a one-point measurement is valid at low to moderate void fraction. Moreover, even if the measurement of the far field subjected to the conditional presence of a bubble is taken just in a vertical direction, it is nevertheless representative of an average over the whole interstitial space around the bubble. This is because the average is taken in a region where the positions of the bubbles are quite random. The distribution of the bubbles is not strictly speaking random, but there is no long-range order. Indeed, we have estimated, from optical fibre probe signals, the pair-probability density $P(r)$ for finding two bubbles separated by a distance r in the vertical direction. A local deficit of $P(r)$ to the rear of the test bubble was observed for small r . It is due to hydrodynamic interactions (see Koch 1993 and Cartellier & Riviere 2001 for lower values of Re and α than in the present study). Nevertheless, at large distances, that is in the region where far-field statistics are evaluated, we found that the positions of the bubbles are statistically independent.

In order to measure the far-field statistics, with this methodology one needs to retain some parts of the signal after the filtering of the near-field perturbations. The spatial extent along the measuring direction of this near field including the bubble is $\overline{V}_B(\tau_{cut,d} + \tau_{cut,u}) + d_B$. The mean vertical separation between two bubbles intercepted by the probe is $\lambda_{12)v} = 2d_b/3\alpha$. We can thus measure \overline{U}_{FF} when $\overline{V}_B(\tau_{cut,d} + \tau_{cut,u}) + d_B < \lambda_{12)v}$. Based on our particular choices of $\tau_{cut,d}$ and $\tau_{cut,u}$, this condition is satisfied up to a void fraction of about 10 %.

4. Experimental results and discussion

4.1. Characteristic length scales of the flow around a bubble

In a bubble swarm, Risso & Ellingsen (2002) showed that, up to a void fraction of 1 %, the velocity of the liquid in the region close to the bubble is similar to the one observed for an isolated bubble (at distances less than $2.5d_B$): it is potential at the front of the bubble and controlled by the wake at the back. They have also shown experimentally that, at low void fraction, the hydrodynamic interactions make the liquid velocity decrease faster downstream of a bubble in a suspension than in the wake of an isolated bubble. In the present work, these results are extended up to $\alpha = 13$ %.

Some general features of the velocity perturbation around the bubbles can be observed for all void fractions. One observes an asymmetry between the flow upstream and downstream of the bubble resulting in different values of the interface velocities and of the relaxation lengths (figure 8). The mean velocities at the interfaces on each side differ from the bubble velocity. This is a result of the averaging process that cumulates interfacial velocities sampled over all the front (or rear) surface intercepted by the probe. The vertical velocity being non-uniform along the bubble interface, the averaged velocities $\langle \tilde{u}(\tau = 0) \rangle_u$ and $\langle \tilde{u}(\tau = 0) \rangle_d$ differ from the bubble velocity. For an isolated ellipsoidal bubble at high Reynolds number a potential velocity field develops at the front the bubble and a wake behind. And in the vicinity of the interface, the vertical velocity along the curvature decreases faster on the potential flow side than on the wake side, as predicted by axisymmetric direct numerical simulations (Ellingsen 1998). This is expected to be also the case close to the interface of a bubble in a swarm. Because the probability of piercing by the probe increases with the distance r from the stagnation point, $\langle \tilde{u}(\tau = 0) \rangle_u$ is smaller than $\langle \tilde{u}(\tau = 0) \rangle_d$. In all of our runs,

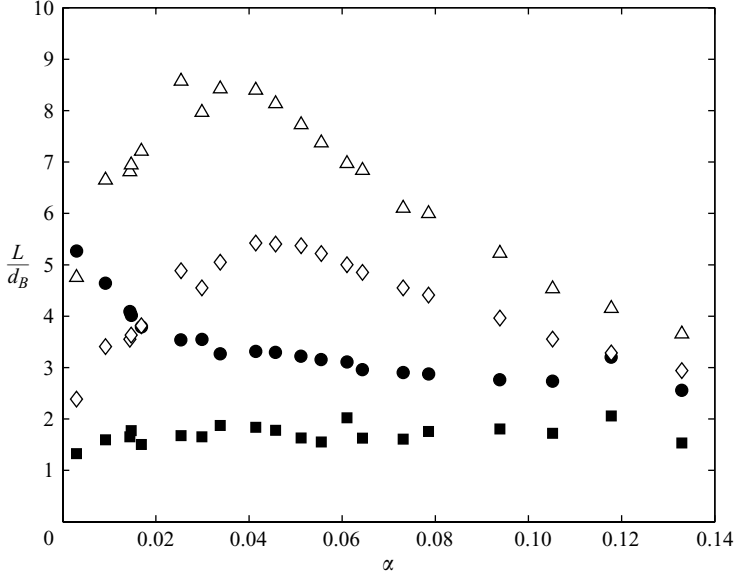


FIGURE 9. Non-dimensional length scales characteristic of the decay of the velocity around a bubble in the swarm: ●, length of downstream perturbation (measurements) λ_{rd}^* ; ■, upstream relaxation length (measurements) λ_{ru}^* ; △, ◇, characteristic length of decay due to multi-body interactions L_{C_D}/d_B , solution of $\langle u_w(L_{C_D}) \rangle / U_R = 0.05$ (see (4.4)). (△, $Re_t = 20$; ◇, $Re_t = 10$).

the characteristic length scale over which the velocity decays downstream of each bubble is much larger than upstream due to the presence of a wake.

Our experimental measurements also show that the velocity perturbation in the wake decays faster in the swarm than for an isolated bubble. This effect is stronger when α increases (figure 8). For all the void fractions, the experimental filtered averaged time series (upstream and downstream) are very well fitted by an exponential law of the form

$$\langle \tilde{u}(\tau) \rangle = U_1 \exp(-|\tau|/\tau_2) + \langle \tilde{u}(\tau \rightarrow \pm\infty) \rangle \quad (4.1)$$

where U_1 and τ_2 are obtained from the fit as functions of α .

The fitted exponential laws enable us to define relaxation times τ_r (τ_{rd} for the downstream average and τ_{ru} for the upstream average respectively) as the times required to satisfy

$$\frac{\langle \tilde{u}(\tau_r) \rangle - \langle \tilde{u}(\tau \rightarrow \pm\infty) \rangle}{\overline{V_B} - \langle \tilde{u}(\tau \rightarrow \pm\infty) \rangle} = \beta = 0.05. \quad (4.2)$$

The associated relaxation length in the wake $\lambda_{rd} = \tau_{rd} \overline{V_B}$ is plotted on figure 9 in non-dimensional form. We thus give evidence of the reduction of the length of the wakes when α increases up to moderate void fractions of about 13%. At low void fraction, the order of magnitude of $\lambda_{rd}^* = \tau_{rd} \overline{V_B} / d_B$ is in agreement with the estimation of the distance necessary to reach an external asymptotic field far away from the bubble made by Risso & Ellingsen (2002) (typically $5d_B$). We are thus confident in the ability of our methodology to characterize the extent of the perturbation induced in the liquid by bubbles passages. The relaxation length in the upstream region $\lambda_{ru} = \tau_{ru} \overline{V_B}$ is also reported on figure 9. This length scale is lower than the wake length and is insensitive to void fraction effects. For any void fraction, the measured value of λ_{ru} has the same order of magnitude as the one we can estimate

from a conditional average of the analytical axisymmetric irrotational flow around an isolated bubble of equivalent diameter. Taking the average over the vertical cylinder intercepting the bubble the predicted value of λ_{ru} is $0.75d_B$, in agreement with the measurements. We thus have an experimental observation of the persistence of the blocking potential flow upstream of a bubble in a swarm.

In the general case, the faster decay rate of the conditionally averaged velocity disturbance in the wake of a bubble in a swarm, compared to an isolated bubble, may result from different screening mechanisms. Among them, as shown by Koch (1993), is that the wake may be modified by the buoyancy due to non-uniform bubble number density and also, whatever the statistical distribution of the bubbles, by the unsteadiness and Reynolds stresses induced by the surrounding bubbles. Two important elementary possible mechanisms have been identified for the surrounding bubbles to distort the velocity field and lead to a rapid disappearance of the wakes at high Reynolds number: external straining exerted on the wake due to the blocking by neighbouring bodies (Hunt & Eames 2002), and wake intermingling between neighbours (White & Nepf 2003; Eames *et al.* 2004), the second mechanism dominating.

In our experimental study, the flow is very complex, due to non-negligible void fraction, three-dimensional free motions of the bubbles, and an inertial regime. We observed at the micro-scale an exclusion zone at the rear of the bubbles, but the spatial extent of this zone λ_{ex} does not scale as predicted by the model of Koch (1993) (we observed with an optical fibre probe $\lambda_{ex} \approx 0.9d_B\alpha^{-0.4}$). However, our void fraction and Reynolds number values are too high to allow a successful detailed comparison with this model as they induce a strong modification of the initial laminar Oseen wake assumed in the model. In our flow, like in Koch (1993), lift forces may contribute to a screening effect by rejecting the bubbles outside the wake of the test bubble, but neighbouring bubbles may also disturb the wake directly, even in the near region, due to the mechanism of wake intermingling. In the following we discuss how, due to the latter mechanism, a screening effect may be observed. We assume a uniform distribution of the bubbles, and discard, due to its complexity, the more realistic problem that requires the coupled resolution of the spatial distribution of the bubbles and of the modification of the test-bubble wake. We examine how the conditionally averaged time series in the wake can be related approximately to an exponential law. We also discuss the origin of an approximate exponential form for $\langle \tilde{u}(\tau) \rangle_u$ in the potential part of the flow. We then compare typical length scales of the wakes measured in the experiments with the values predicted by a model taking into account wake interactions.

In a dilute random assemblage of particles embedded in a uniform flow, the conditionally averaged velocity field around a test particle may be seen as governed by a momentum equation with a distributed sink term associated with the uniformly smeared contributions of the localized forces exerted by the other particles (Koch & Brady 1985). Taking into account only the drag force for the sink term, and assuming that the far wake still has a thin structure, one can solve the momentum equation after linearization of the inertial term. Such an analysis reproduces the effects of wake intermingling as in White & Nepf (2003). But of course it does not represent the coupled problem of free particles moving in a field of intermingling wakes. We have applied this schematic analysis to a random array of spheres, and we have estimated the velocity disturbance u_w of the axisymmetric wake of a bubble in the array:

$$\frac{u_w(x, r)}{U_R} = \frac{Re_t}{32} C_D \frac{d_B}{x} \exp\left(-\frac{Re_t}{4} \frac{r^2}{x d_B}\right) \exp\left(-\frac{3}{2} \frac{\alpha C_D}{d_B} x\right) \quad (4.3)$$

where r and x are the radial and longitudinal coordinates, C_D is the drag coefficient, U_R the relative velocity and Re_t the effective or turbulent Reynolds number in the wake, defined as $U_R d_B / (\nu + \nu_t)$, where ν_t takes into account turbulence effects in the wake. One can recognize in this solution the combination of the solution for an axisymmetric wake of an isolated body (Batchelor 1967) and a second exponential function that includes the attenuation due to the drag array. Thus the perturbation in the wake of a bubble in a swarm may decay rapidly due to wake interactions.

The conditional average given by this model thus can be written

$$\frac{\langle u_w(x) \rangle}{U_R} = \frac{4}{\pi d_B^2} \int_0^{d_B/2} 2\pi r \frac{u_w}{U_R} dr = \frac{C_D}{2} \left(1 - \exp\left(-\frac{Re_t d_B}{16 x}\right) \right) \exp\left(-\frac{3 \alpha C_D}{2 d_B} x\right). \quad (4.4)$$

The upper limit of integration is defined in order to compare to the experimental average related to the detection of the bubble by a probe. This calculation shows that close to the bubble an exponential approximation is expected for $\langle u_w(x) \rangle$. An exponential decay of the experimental downstream averaged velocity $\langle \tilde{u}(\tau) \rangle_d$ is thus predicted in the vicinity of a bubble due to the influence of the neighbouring bubbles on the wake of the test bubble.

We now present a comparison of our measurements with the prediction of a length scale L_{C_D} characteristic of the decay described by (4.4). We define L_{C_D} such that $\langle u_w(L_{C_D}) \rangle / U_R = 0.05$. Assuming an equilibrium between the drag force and the buoyancy, we can estimate approximately $C_D = \frac{4}{3} g d_B / U_R^2$, where g is the acceleration due to gravity. For quite low values of Re_t (10 to 20), there is a reasonable agreement between the orders of magnitude of λ_{rd} and of the predicted value L_{C_D} (figure 9). A better agreement seems difficult to achieve because of the singular behaviour of the wakes that have finite sizes at $x=0$. From the reasonable agreement between the experiments and the model we can infer that multi-body interactions are involved in the wake annihilation in the swarm. Nevertheless, the transverse oscillatory motions induced by the surrounding bubbles may also contribute to the rapid destruction of the wake (Risso & Legendre 2003). The presence of oscillatory motions could explain why low values of Re_t are needed in the model to recover the experimental results.

In the experiments, an exponential decay is also observed in the upstream potential part of the flow. In the conditional averaging process, the random instantaneous trajectories induce random positions of the piercing relative to the positions of the centre of the bubbles, and a random angle between their velocity and the direction of measurement. Moreover, the bubble diameter is not unique as it varies around its mean value, and is a supplementary random variable. The statistical distribution of arrivals of the bubbles, and the fact that the conditional average process mixes the different effects of the various random mechanisms may explain the upstream exponential form, otherwise unexplained. This idea was tested by calculating the global conditional average of the analytic solution of the vertical velocity in a potential flow around a spherical bubble. We have tested first a uniform probability of piercing, and secondly a probability given by the eccentricity of the probe relative to the bubble centre, discarding in this case the extreme eccentricity. These calculations gave a conditionally averaged series that was approximately exponential near the bubbles, but that reverted to an algebraic decay far upstream.

4.2. Mean velocities and relative velocity

In this section we briefly discuss the physical meanings and the links between the various definitions of the averaged velocities. These definitions are recalled in table 1.

Notation	Definition	Significance
$\overline{U_f}$	(3.1)	averaged velocity of the liquid phase
$\overline{V_B}$	(3.2)	statistical mean velocity of the bubbles
$\overline{U_G}$	(3.3)	averaged velocity of the gas phase
$\langle u(\tau) \rangle_d$ and $\langle u(\tau) \rangle_u$	(3.4) and (3.5)	<i>unfiltered</i> conditionally averaged time series of the velocity in the liquid
$\langle \tilde{u}(\tau) \rangle_d$ and $\langle \tilde{u}(\tau) \rangle_u$	(3.6) and (3.7)	<i>filtered</i> conditionally averaged time series of the velocity in the liquid
$\overline{U_{FF}}$	(3.8)	conditional average of the velocity of the liquid in the far field

TABLE 1. Definitions of velocity averages

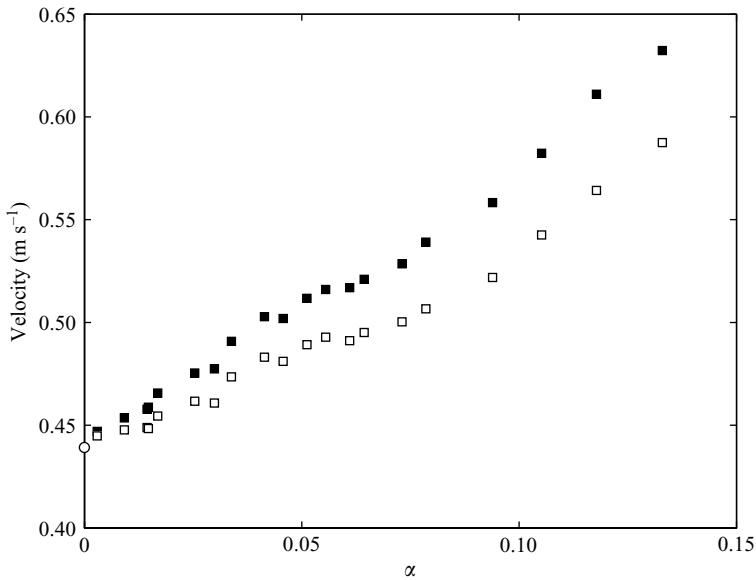


FIGURE 10. Mean velocities of the liquid phase obtained from conditional and non-conditional averages. ■, $\overline{U_f}$ phase average; □, $\overline{U_{FF}}$ conditional average in the far-field; ○, single-phase flow.

In our experiments the absolute velocity of the bubbles is quite insensitive to the void fraction (with data scattering it ranges between 0.6 and 0.64 m s⁻¹).

The mean velocity of the liquid $\overline{U_f}$ increases with the void fraction (figure 10). This is due to the experimental procedure used to vary the void fraction between each run. For a given liquid flow rate, adding a gas flow rate generates an increase in the liquid velocity simply to satisfy mass conservation. At the point of measurement, due to the non-uniformity of the flow associated with the boundary layer development, we could not obtain a perfectly constant local superficial velocity $U = (1 - \alpha)\overline{U_f}$. We thus do not satisfy exactly in a local sense the simple mass balance $\overline{U_f} = \overline{U_{f0}}/(1 - \alpha)$ with $\overline{U_{f0}}$ a constant velocity equal to the velocity in single-phase flow. But this relation mostly explains the dependence of $\overline{U_f}$ upon α .

The conditional averages defined in the far field, $\overline{U_{FF}}$, also evolve with α because they are also sensitive to the global velocity enhancement due to gas injection (figure 10). At low void fraction, $\overline{U_{FF}}$ is very close to $\overline{U_f}$, because, due to the small

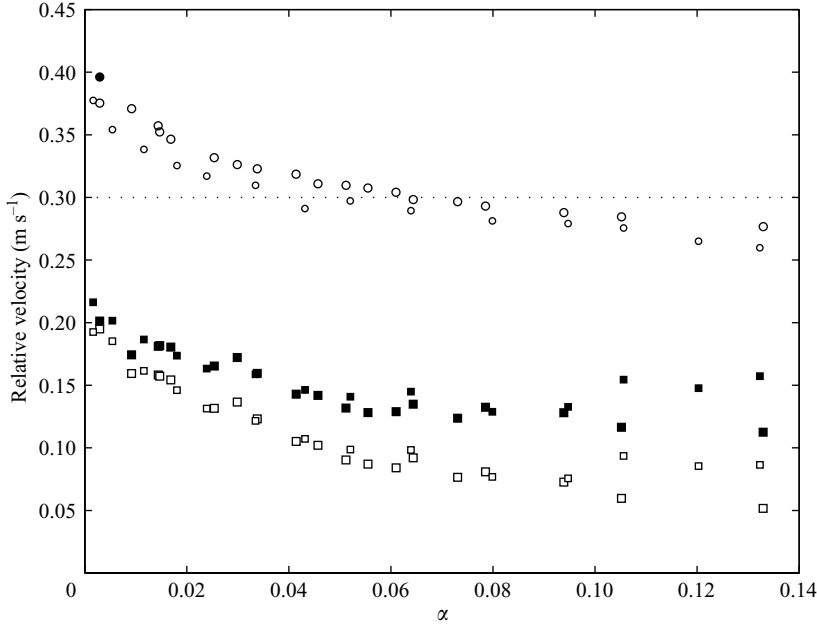


FIGURE 11. Relative velocities of the bubbles: \blacklozenge , U_{RFF} ; \square , U_{RL} ; (large symbols: $x = 17$ cm, $y = 8$ cm; small symbols: $x = 60$ cm, $y = 5$ cm); \circ , terminal velocity from Clift *et al.* (1978) in ms^{-1} : $U_{R\infty} = (2.14\sigma/\rho_L d_B + 0.505gd_B)^{0.5}$, for deformed bubbles with $d_B > 1.3$ mm.

number of bubbles by unit volume, the near field fraction is negligible. For void fractions higher than 10 % there are essentially bubble-induced local perturbations and the liquid is mainly contained in a very thin region between neighbouring bubbles. Such interstitial regions can no longer be considered as far away from *any* bubble. Thus, for high void fractions, a conditional near-field average as well as \overline{U}_f are the pertinent velocity scales. It remains that, for intermediate void fractions, \overline{U}_{FF} still signifies of a large number of statistical events in the liquid. In bubbly flows at moderate void fraction, both velocities \overline{U}_f and \overline{U}_{FF} may thus be useful in discussing and scaling the results.

The relative velocity of the bubbles being at the origin of any motion induced in the liquid, it is fundamental to define it precisely and to examine its dependence upon the flow conditions. Two definitions of the mean relative velocity can be introduced. The first is linked to phase averages, $U_{RL} = \overline{U_G} - \overline{U}_f$, and the second is $U_{RFF} = \overline{V_B} - \overline{U}_{FF}$. Our experimental results show that the difference between U_{RL} and U_{RFF} is noticeable (figure 11). Due to the effect of fluid displacement in the vicinity of the bubbles, U_{RL} is always lower than U_{RFF} . Above $\alpha = 5\%$ or 6% , their difference is at least equal to 30 %. It is thus important to distinguish between these definitions. While U_{RL} is commonly used, U_{RFF} is a definition that better scales the individual relative movement as can be seen on figure 8 where $(\langle \tilde{u}(\tau \rightarrow 0) \rangle_d - \overline{U}_{FF})$ is nearly equal to U_{RFF} . Both relative velocities U_{RL} and U_{RFF} are very different from the terminal velocities $U_{R\infty}$ of bubbles of equivalent diameters (given for example by Clift, Grace & Weber 1978) (figure 11). At very low void fraction we measured a noticeable difference with $U_{R\infty}$, which has never been explained to our knowledge, but has also been observed by van Wijngaarden & Kapteyn (1990) and by Zenit *et al.* (2001). Then both relative velocities U_{RL} and U_{RFF} decrease when the void fraction increases as already observed in several

experiments (van Wijngaarden & Kapteyn 1990; Zenit *et al.* 2001; Garnier *et al.* 2002; among others). Such a reduction of the relative movement is due to bubble interactions, occurring for all the particle Reynolds number, but depending on this Reynolds number (Spelt & Sangani 1998; Esmaeeli & Tryggvason 1998, 1999; Legendre *et al.* 2003). The dependence of U_{RFF} upon the void fraction is different from that of U_{RL} . It reveals that the investigation of a scaling of the relative movement versus the void fraction needs primarily to be based on a precise definition of the relative velocity. In this work we did not attempt to determine such a scaling because the shapes and terminal velocities varied in too large a range and were not determined precisely enough.

4.3. Comparison of interstitial velocity between bubbles with potential flow models

The definition of our far-field conditional average based on signal-processing recovers characteristics similar to the interstitial mean velocity defined by Eames *et al.* (2004) who have proposed new concepts useful for the calculation of the averaged flow created by a bubble swarm. They described the averaged collective effect of the bubbles that modifies the mean liquid flow of a homogeneous flow in the potential approximation. While they defined the Eulerian mean velocity \overline{U}_f as an average over the volume occupied by the fluid in the control volume, the interstitial Eulerian mean velocity (denoted U_E^I in their work) was defined as an average over the total volume occupied by the bubbly region of an asymptotic form of the potential flow. This potential flow is valid in the swarm in the region far from any body. Its definition thus requires a separation of the length scales between the velocity field local to each body and the velocity field far from each body and is thus limited to dilute suspensions. The asymptotic velocity potential associated with each body is thus modelled as a dipole contribution with a dipole moment equal to the moment of an isolated body in a purely potential flow, $4\pi\mu_i = -(1 + C_M)(\overline{V}_B - U_E^I)V_b$ (Taylor 1928) (where C_M is the added-mass coefficient of the bubbles, \overline{V}_B the velocity of the body and V_b the volume of the body). The total asymptotic velocity potential is the sum of all the dipola. Eames *et al.* (2004) have also pointed out a noticeable modification of the flow due to kinematic boundary conditions related to the continuous injection of a dispersed phase at the entrance of a channel.

They have demonstrated that the local superficial velocity U of the liquid is related to the interstitial velocity U_E^I through the following relation where we have replaced U_E^I by \overline{U}_{FF} because both are identically defined far away from any bubble, at least at low void fraction:

$$\overline{U}_{FF} = U - \alpha C_M (\overline{V}_B - \overline{U}_{FF}). \quad (4.5)$$

For bounded channel flows, the local superficial velocity of the liquid U can be calculated from the measured Eulerian mean velocity \overline{U}_f because the mass conservation gives $U = (1 - \alpha)\overline{U}_f$. The added-mass coefficient of the bubbles is estimated for an oblate ellipsoidal bubble in potential flow to be (Lamb 1932):

$$C_M = \alpha_0 / (2 - \alpha_0) \quad (4.6)$$

with

$$\alpha_0 = \frac{2}{e^2} \left[1 - \frac{\sqrt{1 - e^2}}{e} \arcsin(e) \right] \text{ and } e = \frac{\sqrt{\chi^2 - 1}}{\chi}.$$

We used this relation in combination with the aspect ratio χ given by Duineveld (1995) to estimate the added-mass coefficient of the bubbles.

Figure 12 shows the experimental measurements of $(U - \overline{U}_{FF})/(\overline{V}_B - \overline{U}_{FF})$ as a function of α . According to (4.5) it should evolve as αC_M . Experimental results

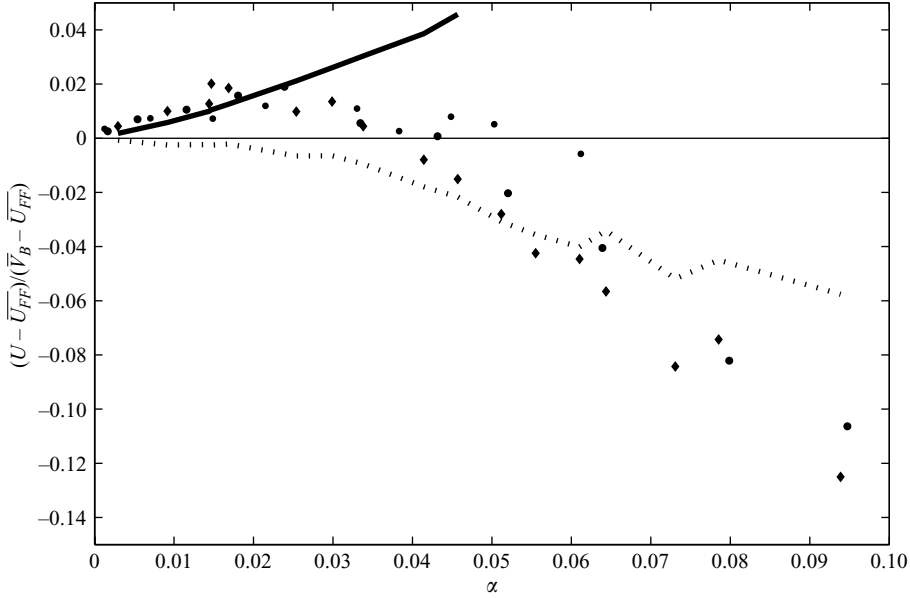


FIGURE 12. Comparison between drift models and experimental results. Experimental results: \blacklozenge , $x = 17$ cm, $y = 8$ cm, $\overline{U}_{f0} = 0.44$ m s $^{-1}$; \bullet , $x = 60$ cm, $y = 5$ cm, $\overline{U}_{f0} = 0.44$ m s $^{-1}$; \circ , $x = 60$ cm, $y = 5$ cm, $\overline{U}_{f0} = 0.3$ m s $^{-1}$. Models: continuous line: model of Eames *et al.* (2004) with $C_M(d_B)$ given by (4.6) and χ given by Duineveld (1995); dotted line: wake modification added to the model of Eames *et al.* (2004) (4.7).

are reported for various locations of the measurement point ($x = 17$ to 60 cm). The experimental curve is insensitive to the location of the measuring region, showing that the degree of homogeneity of the flow is sufficient for comparison with the model. Experimental results are also insensitive to the different values of the mean liquid velocity range explored (0.3 – 0.44 m s $^{-1}$). For low void fraction ($\alpha < 2\%$), the experimental conditions correspond quite closely to the assumptions of the potential flow models: the bubbles are nearly spherical, the Reynolds number is high enough, and the deviation of their motion from rectilinear and stationary path is not important. Moreover, there is a clear separation between the extent of the near field and the extent of the far field. Therefore, even if in our experiments the flow around the bubble is not potential, the approximation of a potential flow around spheres moving at a constant uniform velocity is nearly sufficient to describe the average interstitial field. The potential model gives an interesting insight, because close to the bubble the kinematic effect of the bubble (i.e. the flow around it) dominates the flow pattern (even if it has an attached wake). It is only one or two diameters downstream that the shed vorticity becomes important. Thus the local flux is dominated by a potential flow description. The agreement with (4.5) is noteworthy. It shows that, at low enough void fraction, in agreement with the experiments, U is higher than \overline{U}_{FF} . The experimental results deviate from the potential model of Eames *et al.* (2004) (equation (4.5)) for $\alpha \geq 2\%$. The deviation is linked to effects not taken into account in the model, such as the presence of vorticity, the unsteady motions of the bubbles, and a more approximate separation between the near field and the far field for moderate void fraction. The importance of vorticity becomes more crucial with increasing void fraction, even at

large distances from the bubbles, and the potential flow approximation is less and less valid. This is explored in the next section.

4.4. Discussion of wakes effects

To account for the influence of the vorticity shed by the bubbles on the interstitial flow, it would be necessary to extend the model of Eames *et al.* (2004). This is beyond the scope of the present study. But we can analyse qualitatively the importance of the transport of liquid by the wakes.

To understand the deviation between the experimental results and the predictions of the model, the differences between the concept of interstitial velocity in the potential flow model and our definition of $\overline{U_{FF}}$ must be analysed in detail, since at high α the distinction between a near and a far field is blurred. The model requires a strict separation between the scales of the bubble diameter and of the mean distance between two bubbles. When the void fraction increases, but remains moderate ($\alpha < 8\%$), an asymptotic experimental far field still exists as shown in §3.2.2. Nevertheless its spatial extent is reduced, and for $\alpha \approx 8\%$ the mean distance between two bubbles and the length of attenuation of the wake become comparable, so that there is no longer a separation of lengths. The concept of interstitial velocity introduced by Eames *et al.* (2004) and our definition of a far field thus diverge more and more as the void fraction increases. In the range of moderate void fraction (typically between 2% and 8%) where it is possible to distinguish in the experiments between the near field and the far field, the vorticity shed by the wakes contaminates the far field. A potential approximation for the far field is therefore no longer sufficient. Some fluid in the interstitial zone is transported in the wakes, generating an additional upward contribution to the measurement of the far-field velocity $\overline{U_{FF}}$ which increases the right-hand side of (4.5). We can give a qualitative estimation of the finite volume flux of liquid transported upwards by the wakes:

$$\overline{U_{FF}} \approx U - \alpha C_M (\overline{V_B} - \overline{U_{FF}}) - \frac{\alpha}{V_b} F(\alpha) \int_0^{+\infty} Q(x) dx \quad (4.7)$$

where V_b is the bubble volume, $Q(x)$ is the volume flux in a wake and $F(\alpha)$ the fraction of the interstitial volume occupied by wakes. From the experimental observation of an exponential form for the conditional average, we assume that the volume flux in the wake evolves similarly leading to $Q(x) = Q_0 \exp(-x/\overline{V_B} \tau_2)$. The volume flux Q_0 is estimated from a balance between the drag force D and the momentum defect in the wake $\rho Q_0 (\overline{V_B} - \overline{U_{FF}}) = D$ (Betz 1927), and a balance between the drag force and the buoyancy ($D = g(\rho_L - \rho_G) \pi d_B^3 / 6$). For low void fraction, $F(\alpha) \rightarrow 0$ and the potential model of Eames *et al.* (2004) is recovered (equation (4.5)). For high void fractions $F(\alpha)$ increases towards unity and the second term in (equation 4.7) will grow so as to compensate the downward interstitial flow due to inviscid blocking. It is interesting to notice that (equation 4.7) may reproduce the change of sign of $(U - \overline{U_{FF}})/(\overline{V_B} - \overline{U_{FF}})$ when α increases, as observed in the experiments. We have reported the comparison for $F(\alpha) = 1$ in figure 12. The qualitative agreement of the experimental results with this crude model enhances the importance of the transport of liquid due to the wakes in this configuration.

5. Conclusion

We have developed a method for analysing and interpreting the conditional statistics of the velocity in the liquid phase of a bubbly flow. By combining hot-film

measurements and phase discrimination we were able, with a conditional averaging, to measure the perturbation induced in the liquid velocity in the vicinity of a test bubble in a swarm. We thus observed the attenuation of the length of its wake when the void fraction increases. We were also able to define statistics far away from the interfaces accessible from one-point measurements. The method is based on the estimation of the relaxation regions of the perturbations induced by bubble passages. The far-field statistics, being calculated in a region where the spatial distribution of the bubbles is uniform, are representative of the global dynamics of the interstitial liquid. This method enables current models of the interstitial velocity to be tested. Our definition of an interstitial average, even though it is introduced on signal processing grounds, is consistent with these models. The drift concept and models which up to now have been tested in relatively pure situations (isolated two-dimensional bubbles without open trailing wakes (Bush & Eames 1998)) have been examined in this work in a more complex situation. We have considered the rise of a uniform suspension of many bubbles. While, at low void fraction, we found very good agreement between our experimental results and the potential flow model developed by Eames *et al.* (2004), at higher void fraction the influence of a rotational component of the flow is pronounced. To include the influence of wakes intermingling with their neighbours, and to provide better agreement for higher void fraction, we proposed an approximate correction, but more fundamental work is needed. The examination of the far-field statistical moments of higher order than the unconditional statistics will allow us in future to discuss the near-field and far-field fluctuations of the velocity of the liquid subjected to different mechanisms of generation and transport. Also, it would be interesting to extend this methodology to spatial information about velocity field. The diagnostic techniques developed provide a possible methodology for understanding high void fraction flows, or flows around groups of bodies, such as in urban environments.

Véronique Roig would like to thank Ian Eames for many interesting discussions on this research. This work was partly supported by an EEC Brite-EuRam project, ref. no. BE 4322.

REFERENCES

- BATCHELOR, G. K. 1967 *An Introduction to Fluid Dynamics*. Cambridge University Press.
- BATCHELOR, G. K. 1972 Sedimentation in dilute dispersions of spheres. *J. Fluid Mech.* **52**, 245–268.
- BETZ, A. 1927 Ein Verfahren zur direkten Ermittlung des Profilwiderstandes. *Z. Flugtech. Motorluftschiffahrt* **16**, 42.
- BIESHEUVEL, A. & VAN WIJNGAARDEN, L. 1984 Two-phase flow equations for a dilute dispersion of gas bubbles in liquid. *J. Fluid Mech.* **148**, 301–318.
- BRUUN, H. H. 1995 *Hot-wire anemometry, Principles and signal analysis*. Oxford University Press.
- BUSH, J. W. M. & EAMES, I. 1998 Fluid displacement by high Reynolds number bubble motion in a thin gap. *Intl J. Multiphase Flow* **24**, 411–430.
- CARTELLIER, A. & RIVIERE, N. 2001 Bubble-induced agitation and microstructure in uniform bubbly flows at small to moderate particule Reynolds numbers. *Phys. Fluids* **13**, 2165–2181.
- CLARK, N. N. & TURTON, R. 1988 Chord length distributions related to bubble size distributions in multiphase flows. *Intl J. Multiphase Flow* **14**, 413–424.
- CLIFT, R., GRACE, J. R. & WEBER, M. E. 1978 *Bubbles, Drops and Particles*. Academic Press.
- DUINEVELD, P. C. 1995 The rise velocity and shape of bubbles in pure water at high Reynolds number. *J. Fluid Mech.* **292**, 325–332.
- DREW, D. A. 1983 Mathematical modeling of two-phase flow. *Annu. Rev. Fluid Mech.* **15**, 261–291.
- EAMES, I., BELCHER, S. E. & HUNT, J. C. R. 1994 Drift, partial drift and Darwin's proposition. *J. Fluid Mech.* **275**, 201–223.
- EAMES, I., HUNT, J. C. R. & BELCHER, S. E. 2004 Inviscid mean flow through and around groups of bodies. *J. Fluid Mech.* **515**, 371–389.

- EAMES, I., ROIG, V., HUNT, J. C. R. & BELCHER, S. E. 2004 Vorticity annihilation and inviscid blocking in multibody flows. *NATO meeting, Ukraine, May 2004*.
- ELLINGSEN, K. 1998 Hydrodynamique des écoulements pilotés par l'ascension de bulles d'air virevoltantes. PhD Dissertation, Institut National Polytechnique de Toulouse.
- ELLINGSEN, K. & RISSO, F. 2001 On the rise of an ellipsoidal bubble in water : oscillatory paths and liquid-induced velocity. *J. Fluid Mech.* **440**, 235–268.
- ELLINGSEN, K., RISSO, F., ROIG, V. & SUZANNE, C. 1997 Improvements of velocity measurements in bubbly flows by comparison of simultaneous hot-film and laser-Doppler anemometry signals. *Proc. ASME Fluid Engng Div. Summer Meeting*, Vancouver, Canada, paper 97-3529.
- ESMAEELI, A. & TRYGGVASON, G. 1998 Direct numerical simulations of bubbly flows. Part 1. Low Reynolds number arrays. *J. Fluid Mech.* **377**, 313–345.
- ESMAEELI, A. & TRYGGVASON, G. 1999 Direct numerical simulations of bubbly flows. Part 2. Moderate Reynolds number arrays. *J. Fluid Mech.* **385**, 325–358.
- FARRAR, B., SAMWAYS, A. L., ALI, J. & BRUUN, H. H. 1995 A computer based technique for two-phase flow measurements. *Meas. Sci. Technol.* **6**, 1528–1537.
- GARNIER, C., LANCE, M. & MARIÉ, J. L. 2002 Measurement of local flow characteristics in buoyancy-driven bubbly flow at high void fraction. *Exp. Therm. Fluid Sci.* **26**, 811–815.
- HINZE, J.O. 1987 *Turbulence*. McGraw-Hill.
- HUNT, J. C. R. & EAMES, I. 2002 The disappearance of laminar and turbulent wakes in complex flows. *J. Fluid Mech.* **457**, 111–132.
- KAMP, A. 1996 Ecoulements turbulents à bulles dans une conduite en micropesanteur. PhD Dissertation, Institut National Polytechnique de Toulouse.
- KOCH, D. L. 1993 Hydrodynamic diffusion in dilute sedimenting suspensions at moderate Reynolds numbers. *Phys. Fluids* **5**, 1141–1155.
- KOCH, D. L. & BRADY, J. 1985 Dispersion in fixed beds. *J. Fluid Mech.* **154**, 399–427.
- KOWE, R., HUNT, J. C. R., HUNT, A. & COUET, B. 1988 The effects of bubbles on the volume fluxes and the pressure gradients in unsteady and non-uniform flow of liquids. *Intl J. Multiphase Flow* **14**, 587–606.
- LAMB, H. 1932 *Hydrodynamics*. Dover.
- LARUE DE TOURNEMINE, A. 2001 Etude expérimentale de l'effet du taux de vide en écoulements diphasiques à bulles. PhD Dissertation, Institut National Polytechnique de Toulouse.
- LEGENDRE, D., MAGNAUDET, J. & MOUGIN, G. 2003 Hydrodynamic interactions between two spherical bubbles rising side by side in a viscous liquid. *J. Fluid Mech.* **497**, 133–166.
- RISSO, F. & ELLINGSEN, K. 2002 Velocity fluctuations in a homogeneous dilute dispersion of high-Reynolds-number rising bubbles. *J. Fluid Mech.* **453**, 395–410.
- RISSO, F. & LEGENDRE, D. 2003 Velocity fluctuations induced by high-Reynolds-number rising bubbles : experiments and numerical simulations. *ERCOfTAC Bulletin*, March.
- ROIG, V. 1993 Zones de mélange d'écoulements diphasiques à bulles. PhD Dissertation, Institut National Polytechnique de Toulouse
- SERIZAWA, A., KATAOKA, I. & MICHIOYOSHI, I. 1975 Turbulence structure of air-water bubbly flow. *Intl J. Multiphase Flow* **2**, 221–259.
- SERIZAWA, A., TSUDA, K. & MICHIOYOSHI, I. 1983 Real-time measurements of two-phase flow turbulence using a dual-sensor anemometry. *Proc. Sympo. on Measuring Techniques in Gas-Liquid Two-Phase Flows, Nancy, France*, pp. 495–523.
- SPELT, P. & SANGANI, A. 1998 Properties and averaged equations for flows of bubbly liquids. *Appl. Sci. Res.* **58**, 337–386.
- TAYLOR, G. I. 1928 The energy of a body moving in an infinite fluid with applications to airships. *Proc. R. Soc. Lond. A* **70**, 13–21.
- WHITE, B. L. & NEPF, H. M. 2003 Scalar transport in random cylinder arrays at moderate Reynolds number. *J. Fluid Mech.* **487**, 43–79.
- VAN WIJNGAARDEN, L. & KAPTEYN, C. 1990 Concentration waves in dilute bubble/liquid mixtures. *J. Fluid Mech.* **212**, 111–137.
- ZENIT, R., KOCH, D. L. & SANGANI, A. S. 2001 Measurements of the average properties of a suspension of bubbles rising in a vertical channel. *J. Fluid Mech.* **429**, 307–342.